IEEE Access
Multidisciplinary ⋮ Rapid Review ⋮ Open Access Journal

Received 8 February 2024, accepted 31 March 2024, date of publication 15 April 2024, date of current version 13 May 2024.

*Digital Object Identifier 10.1109/ACCESS.2024.3389074*

APPLIED RESEARCH

# Passive, Fractional, Battery Equivalent-Circuit Model in Time and Frequency Domains Part 1: Linear Model

**VANCE FARROW[1], JONATHAN SCOTT[1], (Life Senior Member, IEEE), MICHAEL J. CREE[1], (Senior Member, IEEE), AND MARCUS WILSON[2]**

[1]School of Engineering, The University of Waikato, Hamilton 3216, New Zealand
[2]School of Science, The University of Waikato, Hamilton 3216, New Zealand

Corresponding author: Vance Farrow (vancef@waikato.ac.nz)

**ABSTRACT** Existing time-domain fractional model simulations of batteries are either limited to short time sequences, frequently less than 100 s, if truly fractional or use low order RC-ladder fractional approximations to reduce computational burden. Here we present an entirely-passive, truly fractional, equivalent-circuit model of a battery. We rely on a Reimann-Louiville fractional order differintegral to account for long time-scales out to 12 days. An analytical solution is provided for the differintegral, subject to the constraint of piecewise constant current. We validate our model fitting against a multi-day sequence of measured time domain data and EIS measured to 10 $\mu$Hz. The spectral content of the current waveform is identified as a crucial factor. The full evaluation of fractional elements leads to residual error of voltage waveforms that is amongst the best in the literature despite the model having only five parameters. In the time-domain, a root-mean-square error (RMSE) as low as 2.8 mV is achieved while maintaining a frequency-domain RMSE of 14 % from measured impedance values over a span of 6 decades. The use of time-weighted regression is shown to be important to the time-domain fit.

**INDEX TERMS** Characterization, electrochemical impedance spectroscopy, equivalent-circuit model, fractional derivatives, rechargeable batteries.

## I. INTRODUCTION

In this manuscript we introduce an entirely passive battery model of exceptional accuracy. By *passive*, we mean that the model does not contain either a dependent or an independent source that can contribute energy to the system. Energy is stored in a fractional capacitor, also known as a constant phase element (CPE) [1]. By this means non-physical addition or removal of energy is completely impossible. Owing to the use of fractional-derivative elements, non-integer differintegrals are required to transfer between frequency and time domains [2]. We introduce this technique using the left-sided Riemann-Liouville definition [3], along with an original analytical solution to expedite computation subject to piecewise-constant stimulus current, see Appendix VII. The model is validated by comparing electrochemical impedance spectroscopy (EIS) data in the frequency domain, and voltage waveform prediction in the time domain. The model can become the heart of a digital twin implementing Self-Tuning Control to track battery State-of-Charge (SoC) and State-of-Health (SoH).

For a battery equivalent circuit model (ECM) to be accepted for use in a digital-twin system, it must be possible to predict terminal voltage given the current with reasonable accuracy. This is not a trivial calculation in the case of an ECM containing CPEs. It is desirable to carry out this calculation analytically for some special cases, even if the general situation demands a numerical solution.

Our approach contributes to knowledge by using a passive fractional ECM that is fit to the measured voltage on a battery due to a piecewise-constant current stimulus. While a seeming limitation, the use of piecewise constant

The associate editor coordinating the review of this manuscript and approving it for publication was Bo Pu.

stimuli not only enables efficient analytical calculation of the Riemann-Liouville differintegrals, but also enables one to draw insightful conclusions about the impedance of batteries, the conditions under which reliable fitting must be performed, and the appearance of non-linearity even in the so-called linear region of battery operation.

In addition, the fit is performed both in the frequency and time domain and each is tested not only back on its signal (which is likely to be favourably biased) but also is used to make predictions in the conjugate domain thereby giving an independent test of the quality of fit. It is this that enables one to make further inferences about the impedance of the battery and necessary conditions when fitting in the time domain.

In this manuscript we restrict to a linear model. This model is satisfactory provided the battery remains above approximately 20% State-of-Charge (SoC). A later manuscript will address the nonlinear case, but is out of scope for this manuscript.

## II. THE STATE OF THE ART

### A. EQUIVALENT-CIRCUIT MODELS

The modern battery model traces its roots to early electrochemical literature. The introduction of the Warburg element in 1899 to model impedance was extended to arbitrary order fractional elements in 1932 [4] and famously employed by Randles in 1947 [5], thus the literatures [6], [7], and [8] has suggested for some time that battery ECMs should be composed of resistors, capacitors, fractional-derivative capacitors and Warburg elements. Batteries are a complex electrochemical system and models that attempt to contain all of the underlying intricacies become impenetrably complex. Westerhoff's model [7], for example, contains nine resistors, two capacitors, three CPEs and two Warburg elements. More contemporary authors have decried the excessive parameters present in many of the more complex battery models in the literature and the lack of focus on accurate parameter identification [9].

Nevertheless, authors since the 1980s have acknowledged that a small subset of this full ECM is expected to be adequate for all practical purposes [6]. Choosing a representative model is a challenge in its own right as models with differing elements and topologies can behave in a similar manner and in practical measurements, with the additional noise and measurement error, become difficult to distinguish [10]. Nevertheless, it has recently been shown that a model containing one resistor and two CPEs in series is sufficient in a wide range of cases [11], and is the model used in this manuscript.

### B. FRACTIONAL CALCULUS

The mathematics of fractional-order calculus has a long history with many of the most famous names in mathematics and science making contributions. This long history also brings with it many options to choose from when deciding on how to model fractional order behavior [12]. The most commonly seen forms in the literature are Grünwald-Letnikov, popular for being intrinsically discrete in nature, easing the implementation of a practical system [13]; Caputo, which allows for traditional initial and boundary conditions to be used when solving problems [14]; and Riemann-Liouville, allowing for arbitrary functions which need not be continuous at the origin or differentiable [14]. In this paper, we use the Riemann-Liouville form.

### C. MODELING CPES

Modeling time-domain fractional order behavior has been the focus of many notable works in the field of filter design. Whether through a more abstract approach of manipulating poles and zeros [15] or through the careful selection of discrete components [16] it becomes clear that a deliberate arrangement is required to properly form a model of fractional-order behavior from simple R-C circuits, leading to large arrays of components but with a very small number of defining parameters. This constraint is not routinely enforced when papers claim fractional inspiration of their battery models by including an R-C ladder circuit, greatly diminishing the interpretability of the fitted model and its underlying fractional parameters.

These fractional parameters have been shown to correlate with battery health [17], [18], [19] and may prove key to the successful implementation of an accurate battery modeling tool. In this manuscript we use the analytical solution of the Riemann-Liouville differintegral presented in the Appendix, thus avoid any need for R-C ECMs.

### D. FITTING AND VALIDATION

There are many papers presenting ECMs for lithium batteries. In this and the following subsection we review recent manuscripts to see how the performance of models is assessed, and the voltage prediction accuracy that is achieved.

A challenge to the success and applicability of common methods is that most, [17], [18] for example, fit entirely to time domain data, and many ''validate'' model parameters by recreating the same data to which they were fitted in the first place. Conversely, Farrow [19] relied entirely on frequency domain measurements, extracting model parameters from a regression to impedance measurements to very low frequencies. These two approaches result in contradictory results as to whether the fractional order has a positive or negative correlation with SoH. The authors of time domain fitting claim that order increases with SoH, yet this implies a corresponding increase in battery efficiency as the fractional-order system comes to more closely resemble an ideal capacitor—a behavior simply not observed in real batteries. In contrast, Farrow [19] claims that fractional order decreases with SoH, close to the observed behavior of real battery systems whereby efficiency decreases with age and wear. Unfortunately, that work lacked the validation of time domain simulations and produced relatively sparse

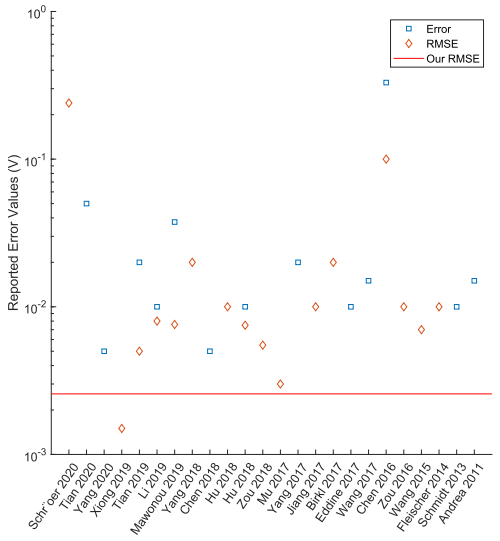


**FIGURE 1. Summary of achieved voltage prediction accuracy in recent literature. The horizontal line indicates the position of the work in this manuscript.**

measurements of impedance due to the complications of making such measurements [19].

Impedance measurements, while time consuming and difficult to make, are considered reliable, yet unsuitable for implementation in practical systems. Time domain fitting of model parameters could solve these issues but has yet to be shown to produce equivalent results in a practical scenario. In this paper we evaluate the convergence between the parameters derived from time domain battery usage data and from frequency-domain battery impedance measurements (EIS) to determine if time domain fitting is a suitable replacement for frequency domain impedance analysis for the extraction of fractional order ECM parameters.

### E. MODEL ACCURACY

A number of relevant papers have been published in the last decade attempting to model battery behavior [13], [18], [20], [21], [22], [23], [24], [25], [26], [27], [28], [29], [30], [31], [32], [33], [34], [35], [36], [37], [38], [39], [40], [41], [42], [43], [44], [45], [46], [47], [48], [49]. Of these 34 manuscripts, 14 report the magnitude error in battery predicted voltage as a function of time as their measure of success. Some 19 present root-mean-square error between expected and predicted voltage. Some 11 present relative error, that is scaled to a fraction or percent, between expected and predicted voltage to evaluate performance. Only two present mean-absolute-error and a further three give mean-relative-error with many authors choosing to provide a combination of measures. Figure 1 summarises the spread for 24 examples with clear numerical statements.

Most models are evaluated through comparison of a predicted and measured variable, usually voltage, on a sample that resembles the data originally used to train the model. This leads to concerns of overfitting and the generality of their proposed models and methods. There are many existing works using fractional order elements for circuit modeling, however due to the nature of the time-domain fractional-order behavior most incorporate either a truncation or an approximation to truly fractional order behavior in favor of drastically reduced computational complexity. While some papers show extensive simulation over long periods, the truncation of the fractional order behavior to a period significantly shorter than this effectively limits the frequency bandwidth which they are able to utilise. In this manuscript we examine the model by comparing predictions across *both* frequency (EIS) and time (I/V) domains over *both* a very long period and very low frequencies as seen in Table 1.

## III. MODEL FITTING

We use the R-CPE-CPE linear circuit model of Poihipi et al. [11], shown in the inset of Fig. 2. A linear model is considered satisfactory for good reason: our EIS data is obtained using a multitone stimulus, and Fourier analysis of the measured voltage waveform shows no intermodulation products.

This model has five parameters, namely the series resistance $R_s$, the constant of proportionality $C_1$ and order $\alpha_1$ of the first CPE, and likewise $C_2$ and $\alpha_2$ for the second CPE. The inclusion of the series resistance and first CPE are easily justified by the presence of the two dominant asymptotic lines of the EIS (see Fig. 2). The second CPE often provides a useful improvement of the fit, particularly in the shape of the curve between the two asymptotes.

First EIS [50], [51] is performed on the test battery cell and the model fitted with the methodology of Poihipi et al. [11] applied in the frequency domain to obtain initial approximations for the parameters of the model (see 'EIS values' row in Table 2).

To fit the model in the time-domain, we choose a suitable current waveform, deliver that current to the battery, and measure the terminal voltage that results. The parameters of the model are estimated by minimising the squared-error between the voltage predicted by the model and that measured. To efficiently and confidently predict the resultant terminal voltage from the current waveform in the time domain, we limit ourselves to piecewise-constant current waveforms so that the resultant voltage can be calculated analytically. Even so, as the number of constant piecewise sections increase, the calculation can quickly become burdensome!

The fitting task is then to choose the five parameter values to obtain the best possible agreement between the predicted and measured terminal voltage waveforms. A multi-parameter gradient descent is used (the nlinfit routine of Matlab which uses a Levenberg-Marquardt algorithm) to adjust the model parameters to minimize the squared error in predicted voltage as seen in Fig. 3. This fitting in the time domain is distinct from the model fitting of the EIS which fits the model parameters in the frequency domain.

**TABLE 1. A sample of existing fractional order modeling papers. These papers were selected for their performance and diversity of approaches to implementing fractional order elements into battery models for parameter extraction. The papers are ordered by increasing computational complexity of their approximations for fractional order behavior.**

| Author | #Parameters | Fractional Model | Time-domain | Frequency-domain | Time/Frequency Span |
|---|---|---|---|---|---|
| Schröer et al. [13] | 8 | 5th Order Approximation | Yes | Yes | 10 s / 10 mHz – 6 kHz |
| Li et al. [34] | 9 | 1 s Truncated Model | Yes | No | 1200 s |
| Xiong et al. [24] | 8 | 40 s Truncated Model | Yes | No | 50000 s |
| Tian et al. [32] | 5 | 100 s Truncated Model | Yes | No | 300 s window |
| Mu et al. [23] | 4 | 500 s Truncated Model | Yes | No | 20000 s |
| This work | 5 | No Truncation | Yes | Yes | 12 Days / 10 $\mu$Hz – 2 Hz |

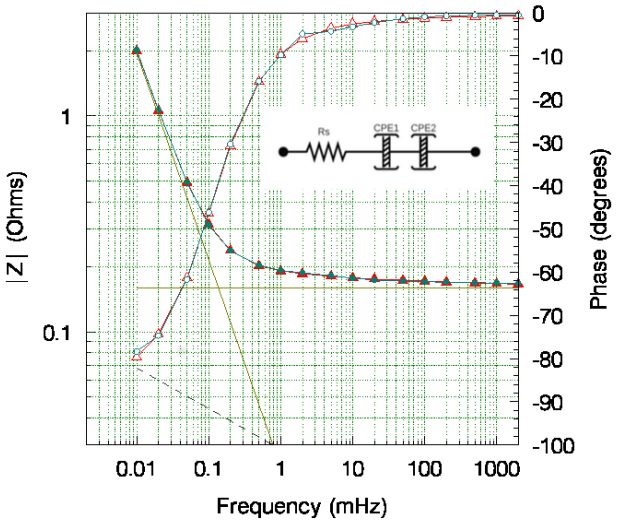


**FIGURE 2. Electro-Impedance Spectrocopy (EIS) magnitude (filled symbols) and phase (open symbols) data measured on the INR 18650 cell (cyan, dots), presented in Bode format, overlayed with the model prediction (red, triangles). The Equivalent-Circuit Model (ECM) is shown as an inset. The straight lines show the impedance of the three elements of the ECM separately.**

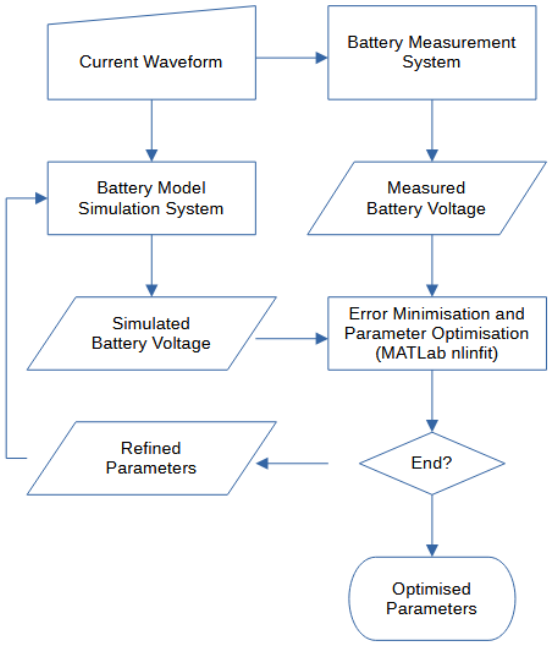


**FIGURE 3. A multi-parameter gradient descent is used to minimise the error between the battery model and the measured voltage to optimise the parameters.**

Two example constant piecewise current waveforms are used in this work. The first is a periodic shallow cycling waveform (see Fig. 4) which consists of few constant sections, thus the time-domain model fitting can be performed very efficiently. This shallow cycling waveform was chosen as a simple proof of concept. As presented below, it was found that fitting to this current stimulus lead to less than desireable results (see 'Time-domain (cycle)' of Table 2 of the Results section) with the series resistance eliminated and the second CPE order reduced almost to that of a resistor, leading to an underestimation of the impedance at higher frequencies (particularly above 100 mHz).

We formulate two plausible explanations for this:

1) the cycling current waveform lacks frequency content, particularly that in the mid-frequency range (0.1–1 mHz) necessary to identify the second CPE;
2) the failure of the model to cope with transient non-linearity evident at large step changes in current, which are dominant in the periodic cycling stimulus but are absent from the multitone stimulus used in EIS.

To address the first, we created a second waveform which is a crude approximation to that which a single cell in a pack might see during usage of an electric vehicle. Fig. 5 presents the stimulus current component of the waveform. The waveform duration is 12 days with stimulus periods randomly spaced but approximately daily, giving frequency content down to 11$\mu$Hz. The current has been set to be constant for durations that are multiples of one minute so that the methods described in Appendix VII can be used to speed up the calculation of the Riemann-Liouville differintegral. The simplified driving waveform is designed to provide a more realistic waveform than the cycle waveform, with increased spectral content at mid and lower frequencies.

To address the possibility that non-linearity may explain the failure to reliably fit the second CPE, a weight function is used in the fitting to de-emphasize the measured voltage points that follow a sudden change in current. The argument is that non-linearity in the battery is most evident immediately

**TABLE 2. Model parameter values.**

| | $R_S$ ($\Omega$) | $\alpha_1$ | $C_1$ | $\alpha_2$ | $C_2$ |
|---|---|---|---|---|---|
| EIS (Frequency-domain) | 0.164 $\pm$0.003 | 0.98 $\pm$0.02 | 6600 $\pm$1100 | 0.26 $\pm$0.07 | 130 $\pm$55 |
| Cycle (Time-domain) | $-$0.2 $\pm$0.1 | 0.9956 $\pm$0.0002 | 8080 $\pm$20 | 0.015 $\pm$0.005 | 3 $\pm$1 |
| Drive (Time-domain) | 0.0889 $\pm$0.0007 | 0.98813 $\pm$0.00003 | 7731 $\pm$3 | 0.0892 $\pm$0.0006 | 15.3 $\pm$0.2 |
| Weighted Drive (Time-domain) | 0.1586 $\pm$0.0003 | 0.98934 $\pm$0.00004 | 7876 $\pm$4 | 0.219 $\pm$0.002 | 88 $\pm$2 |

Notes: Fractional capacitance is in units of $AV^{-1}s^{\alpha}$.
Uncertainty values represent the confidence of the fit, not be confused with predictive performance of the model; values with large uncertainty have lower impact on the time domain voltage.

**TABLE 3. Impedance values.**

| Frequency (Hz) | $1x10^{-5}$ | $2x10^{-5}$ | $5x10^{-5}$ | $1x10^{-4}$ | $2x10^{-4}$ | $5x10^{-4}$ | $1x10^{-3}$ | $2x10^{-3}$ | $5x10^{-3}$ | $1x10^{-2}$ | $2x10^{-2}$ | $5x10^{-2}$ | $1x10^{-1}$ | $2x10^{-1}$ | $5x10^{-1}$ | $1x10^{0}$ | $2x10^{0}$ |
|---|---|---|---|---|---|---|---|---|---|---|---|---|---|---|---|---|---|
| EIS Measured | 2.019 | 1.065 | 0.492 | 0.311 | 0.238 | 0.204 | 0.193 | 0.187 | 0.182 | 0.177 | 0.174 | 0.172 | 0.171 | 0.170 | 0.169 | 0.168 | 0.168 |
| EIS Fit | 2.048 | 1.073 | 0.494 | 0.316 | 0.241 | 0.205 | 0.194 | 0.188 | 0.182 | 0.179 | 0.176 | 0.174 | 0.172 | 0.171 | 0.169 | 0.168 | 0.168 |
| Cycle Fit | 1.907 | 0.974 | 0.428 | 0.264 | 0.199 | 0.170 | 0.162 | 0.157 | 0.152 | 0.148 | 0.144 | 0.139 | 0.136 | 0.132 | 0.128 | 0.124 | 0.121 |
| Drive Fit | 1.877 | 0.978 | 0.455 | 0.300 | 0.236 | 0.205 | 0.194 | 0.186 | 0.178 | 0.172 | 0.167 | 0.161 | 0.157 | 0.153 | 0.148 | 0.144 | 0.141 |
| Weighted Drive | 1.875 | 0.978 | 0.454 | 0.298 | 0.234 | 0.204 | 0.194 | 0.188 | 0.182 | 0.178 | 0.176 | 0.172 | 0.171 | 0.169 | 0.167 | 0.166 | 0.165 |

Impedance of fit model parameters evaluated at the same frequencies where the EIS measurements have been taken

following a large current change. The battery falls out of its usual quasi-static equilibrium, and requires a short period of time to settle back. If measurements immediately following such a change are given less weight when fitting, the non-linearity will not upset the convergence. The weight function is created using a scaled convolution of a one-sided gaussian and the derivative of the current. This ensures the weight function affects only datapoints following a step and the magnitude of the current steps controls the weighting given.

## IV. EXPERIMENTAL METHODOLOGY

All testing was performed on a single lithium-cobalt-oxide (INR) 18650 cell with a rated capacity of 2.5 Ah, with all measurements made at a fixed ambient temperature of 22° C. Tests were carried out using an Agilent 66332A supply controlled through a GPIB interface using custom software running on Raspberry Pi model 4 computers [51].

Fig. 2 shows the EIS data. The impedance measurement was performed using the "bzdcp66" method of [51]. From this, the initial model parameters are obtained. These parameters are used as initial values for the time-domain fitting procedure. Time-domain fitting was carried out in MATLAB running on a 32-core Linux server with 128 Gbytes of RAM.

Fitting was then performed in the time-domain using

1) the shallow cycling dataset of Fig. 4 ('cycle'),
2) the more realistic second waveform of Fig. 5 ('drive'), and
3) the more realistic second waveform, incorporating the weight function to de-emphasize measurements subject to non-linearity ('weighted drive').

The fitted model parameters from all fits are then used to predict the resultant voltage in the time-domain and to predict the resultant impedance in the frequency domain. In this way the EIS-derived model is tested for its ability to predict in the time-domain on the two current sources, and the time-domain derived models are tested for their ability to predict impedance in the frequency domain, thereby better validating the model.

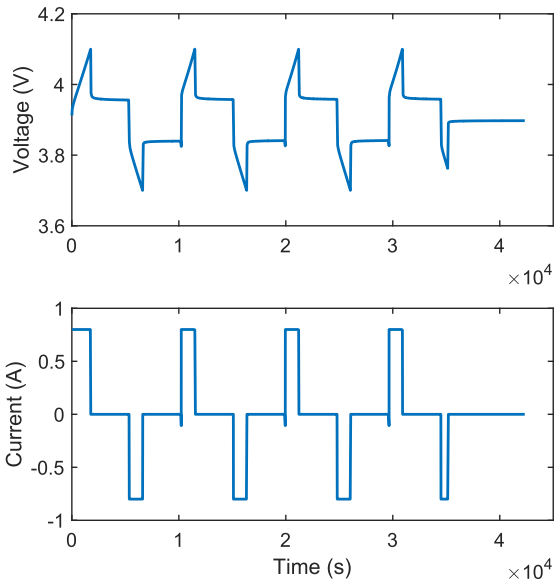


**FIGURE 4. Cycling of the INR 18650 battery. The driving current consists of a series of constant-current pulses and rests, the voltage response is a complex series of transients.**

## V. RESULTS

The EIS data measured on the INR 18650 battery cell is shown in Fig. 2 with the model parameters resulting from the fit in the frequency domain listed as 'EIS values' of Table 2. Straight line asymptotes in Fig. 2 represent the impedances of the individual elements in the equivalent circuit. Time-domain fitting results appear in figures 6, 7, 8, and 9.

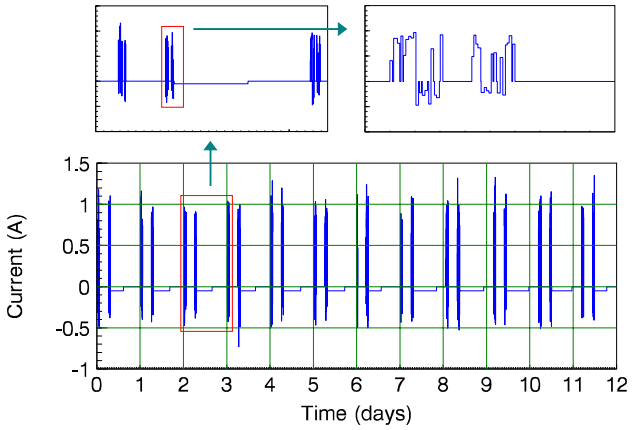


**FIGURE 5.** Plot of the stimulus current representing a simplified version of vehicle current over a 12-day period. The upper two boxes zoom in to expose the details of the waveform.

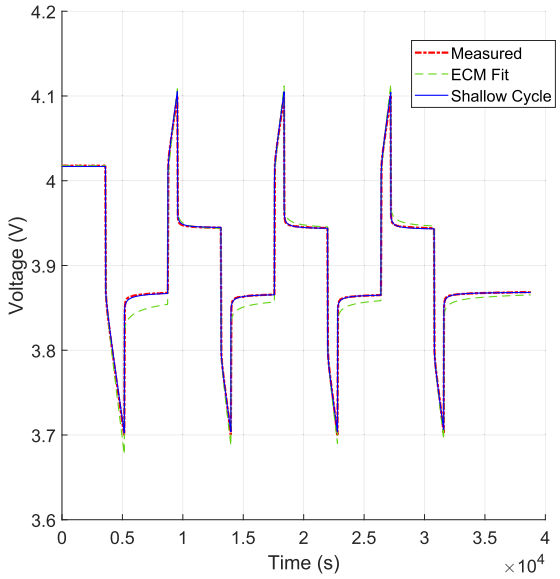


**FIGURE 6.** Measured (red dots) battery terminal voltage is compared with that simulated by the model fitted to EIS data (green dashed line) and to cycle waveforms in the time domain (blue line).

The model parameters resulting from the time-domain fits to the cycle and drive current stimuli on the battery, along with the parameters resulting from the fit to the drive current stimuli with the weight function to de-emphasize regions affected by non-linearity of the battery are also listed in Table 2.

Having derived the model parameters from fitting in the time-domain, it is possible to predict the impedance of the battery in the frequency domain. Plots of the EIS (impedance magnitude spectrum) can include not only the measured data and the prediction from the ECM fitted to the measured EIS data, but can potentially include the prediction from the ECM fitted to the 'cycle' waveform, the prediction from the ECM fitted to the 'drive' waveform, and the prediction from the ECM fitted to the 'weighted drive' waveform with de-emphasized step tails. This provides the additional mechanism for evaluating or validating a parameter set.

Measured and predicted voltage in the time-domain for the cycle current source is shown in Fig. 6, along with the prediction from model parameters derived purely from the fit to EIS data. The model parameters from the time-domain fit on the cycle waveform produces a fit that is remarkably close, despite the fact that the time-domain input contains relatively little information in the lower-frequency range compared with the EIS data. The figure reveals more discrepancy for the EIS fit, something like 20 mV, or 5%. The 'cycle' time-domain fit appears excellent in this instance, but if the results are viewed in the frequency domain a different story appears. Figure 8 presents the EIS results; note that the EIS fit appears superior to the 'cycle' time-domain fit!

Predicted voltage in the time-domain for the case of the 'drive' current source for the model parameters obtained from EIS and from the drive time-domain fits with and without weighting are shown in Fig. 7, again with the measured data. The fits to the time-domain are superior to that derived from EIS. The waveform is more challenging, and the traces do exhibit some minor deviations from the measured data with differences up to 35 mV and an RMSE of 2.8 mV. Looking at the associated EIS plot in figure 9, it can be seen that the weighted fit is superior in both domains. The RMS percent deviation in the impedance calculated from the weighted drive parameters is 14 %, improving on the 32 % of the unweighted drive and 75 % of the shallow cycling parameters.

## VI. DISCUSSION

Figure 6 clearly shows that the time-domain fitted parameters predict the terminal voltage more accurately than the EIS-based parameters. Conversely, figure 8 shows the reverse outcome in the frequency domain, where the time-domain fitted parameters do a poor job of predicting measured data. As discussed previously, the shallow cycle waveform lacks spectral content. This leads to the divergence of the trace approaching 1 Hz.

Figure 7 presents the time-domain results from the more nuanced waveform, and includes results with reduced weighting immediately after step changes. Both time-domain fits improve upon the EIS-based fit. The weighted and unweighted traces disagree only slightly, with the unweighted fit being less accurate after a step change. Consulting the associated EIS data in figure 9 it is clear that the unweighted model parameters deviate significantly at higher frequencies. The inescapable conclusion is that non-linearity, attributed to loss of quasi-static equilibrium, is interfering with the convergence of model parameters. Moving to a waveform with better spectral content alone is not sufficient to cause a dramatic improvement. Accounting for the disturbance with the weighting function yields a significant improvement.

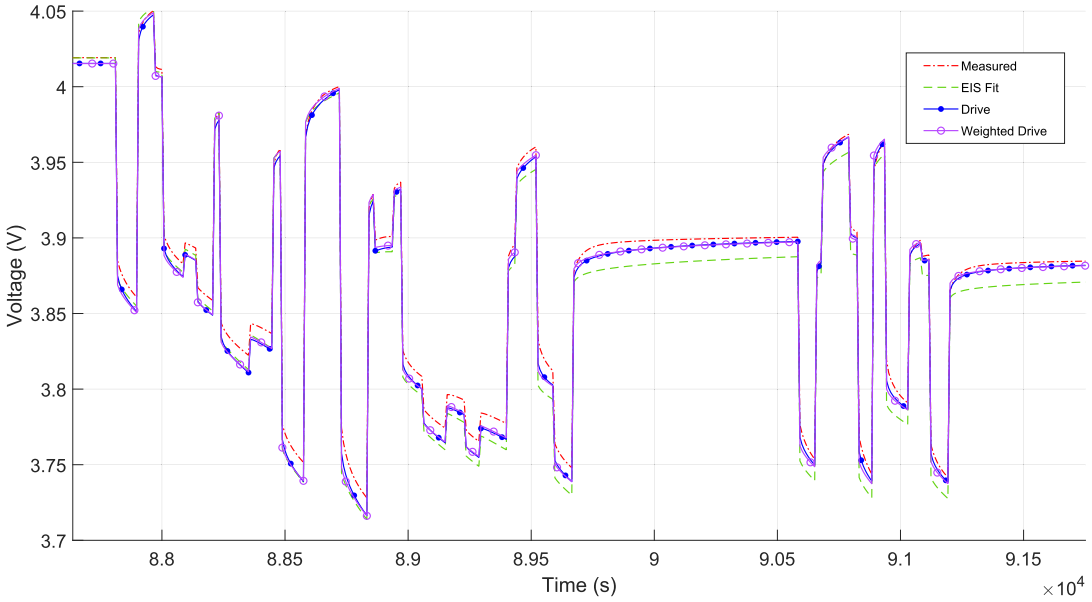


**FIGURE 7.** Zoomed-in view from a section of the drive waveform voltage after model fitting. Measured battery terminal voltage (red dash-dotted line) is compared with prediction from EIS-based model parameters (green dashed line) and time-domain based model parameters with unweighted samples (blue line with dots) and weighted samples (purple line with circles). The latter two lie on top of each other except after step changes, where they can be briefly distinguished.

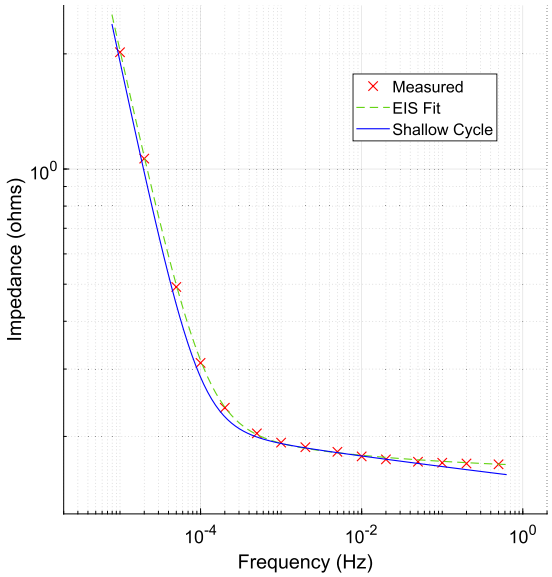


**FIGURE 8.** EIS plot associated with Figure 6. Measured impedance (red symbols), is compared with the impedance from the model fitted to the measured impedance data (green dashed line) and the impedance predicted from the model using parameters obtained from the time-domain fit to the cycle current source (blue line).

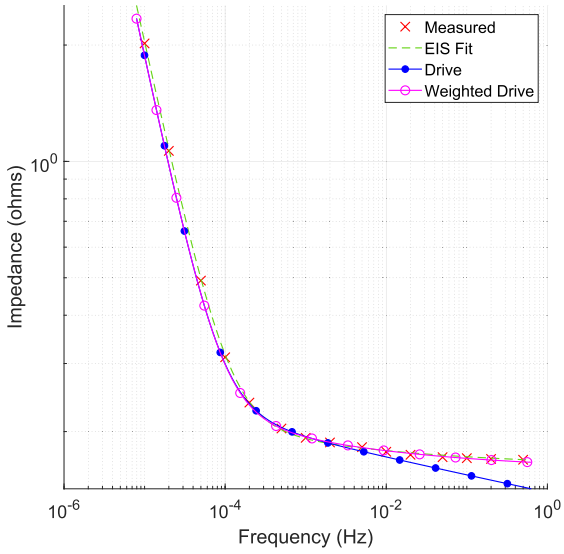


**FIGURE 9.** EIS plot associated with Figure 7. Measured impedance (red crosses) is compared with prediction from EIS-based model parameters (green dashed line) and time-domain based model parameters with unweighted samples (blue line with dots) and weighted samples (purple line with circles).

Overall, the predictive power is excellent, leading to the low RMSE shown in figure 1. It is worth noting that the RMSE is essentially the same in this case of the time-domain waveform for weighted and unweighted fits; it is only when the EIS fit is taken into account that the overfitting of the unweighted method is exposed.

## VII. CONCLUSION AND REFLECTION

In this manuscript we have

1) introduced a passive model, requiring no dependent or independent, current or voltage source, thus guaranteeing charge and energy conservation;
2) dealt with fractional branches using a full differintegral with no assumption of periodicity;

3) presented an analytical solution for the differintegral in the case of piecewise-constant functions;
4) shown this model to provide voltage prediction accuracy amongst the best available in the literature;
5) verified the performance of the model in the frequency domain as well as the time domain;
6) specifically relied upon the extra-low frequency region stretching down to microhertz.

It is interesting to note that 1 above says the impedance model of a battery is equivalent to the complete equivalent-circuit model. This knowledge is essentially implicit in much of the electrochemical literature yet completely alien to authors in the electrical engineering literature. Many authors seem to feel bound to include some source, typically a voltage source reminiscent of a Thévenin circuit. This is inelegant, and proves to be unnecessary. We believe this manuscript is the first formal statement of this.

It has been assumed that the battery remains in the approximately-linear region, often taken as 20%–80% capacity. This assumption is justified by the absence of intermodulation products in the multitone spectrum. The model parameters obtained from the time-domain fitting are somewhat different from the EIS measurements. The conclusion is that the impedance of the battery is different when subjected to the different current waveforms. Recent work explains why this might be the case [52], and how the effect can be minimized in EIS measurements [51].

Electrical engineers do not expect small-signal and large-signal measurements to agree. EIS is implicitly small signal where linearity is assumed to hold, whereas real-world measurements tend to reach large enough current values and charge excursions that non-linear effects begin to appear. A nonlinear extension (Part 2) of this work is underway. It will allow the model to function as the battery excursions take it toward the flat state, and through step changes in current. The non-quasi-static effect gives reason to expect the nonlinear model to converge using data that includes step changes even if the battery is not pulled close to zero state of charge.

## APPENDIX
## ANALYTICAL SOLUTION OF RIEMANN-LIOUVILLE DIFFERINTEGRAL FOR PIECEWISE-CONSTANT CURRENT

In this manuscript we take the Riemann-Liouville (RL) left-sided integral definition [3], [53] of order $\alpha$ from $a$ to time $t$ of the function $f(t)$:

$$I_a^\alpha\{f(t)\} = \frac{1}{\Gamma(\alpha)}\int_a^t (t-\tau)^{\alpha-1} f(\tau)\,d\tau \tag{1}$$

This leads to the equation for the voltage across a CPE conducting a current $i_c(t)$ at time $t = T$:

$$v_{CPE}(T) = \frac{1}{C_F} I_a^\alpha\{i_c(t)\}\,|_{t=T} \tag{2}$$

where $C_F$ is the constant of proportionality sometimes called a "pseudo-capacitance", and the complete history is accounted by allowing $a \to -\infty$.

We commence by "conditioning" the battery. In practice, one might not know the immediate history of the battery, and so we choose a plausible conditioning current that will lead to a reasonably stable terminal voltage of $V_0$ at time $t = t_0$. We choose to condition the battery by applying a constant current at a time $t = t_a \ll 0$ far in the past, and for a short period up to $t_b$, so that the battery has been at rest for some time at the commencement of the experiment:

$$i(t) = I_0[U(t-t_a) - U(t-t_b)] \tag{3}$$

where $U(t)$ is the unit step function, zero for negative time. Combining (3) with (2) and using (1) yields

$$v_{CPE}(t) = \frac{I_0}{C_F\Gamma(\alpha)}\int_{-\infty}^{t} (t-\tau)^{\alpha-1}[U(t-t_a) - U(t-t_b)]\,d\tau \tag{4}$$

and we choose $t_a < t_b \ll 0$ so that

$$v_{CPE}(t)|_{t=0} \approx V_0 \tag{5}$$

which is the desired outcome. The RL integral is not typically analytically tractable for an arbitrary $f(t)$, but we have limited ourselves to constant-amplitude step functions, hence

$$\int_{-\infty}^{t} (t-\tau)^{\alpha-1} U(\tau - t_a)\,d\tau = -\frac{1}{\alpha}U(t-t_a)[(t-\tau)^\alpha]_{t_a}^t = \frac{1}{\alpha}(t-t_a)^\alpha U(t-t_a) \tag{6}$$

can be used with (4) to get

$$v_{CPE}(0) = \frac{I_0}{C_F\Gamma(\alpha+1)}\big[(t-t_a)^\alpha U(t-t_a) - (t-t_b)^\alpha U(t-t_b)\big] \tag{7}$$

and then

$$v_{CPE}(0) = \frac{I_0}{C_F\Gamma(\alpha+1)}\big[(-t_a)^\alpha - (-t_b)^\alpha\big] \tag{8}$$

In this manuscript we need only break the evaluation of $v_{CPE}$ into a sum of terms of the form in (8). As fractional order behavior is still linear, deconstruction of the piecewise constant current waveform into a series of unit step functions allows a simple analytical solution to time domain simulation.

A simple scheme is to apply a current of $I_{ch}$ until $v_{CPE}(t)$ reaches $V_{ch}$ and then a current of $I_{dis}$ until $v_{CPE}(t)$ reaches $V_{dis}$.

$$\begin{aligned} i(t) = I_0\big[&U(t-t_a) - U(t-t_b)\big] \\ &+ U(t-t_0)(I_{ch}) + U(t-t_1)(-I_{ch}) \\ &+ U(t-t_1)I_{dis} + U(t-t_2)(-I_{dis}) \end{aligned} \tag{9}$$

where $t_n < 0$, time $t_0$ and $t_1$ define the charge period, and $t_1$ and $t_2$ the discharge period, chosen to obtain the desired voltage limits. and the terminal voltage of the battery is straightforwardly obtained from

$$V_B(t) = v_{CPE1}(t) + v_{CPE2}(t) + i(t)R_S \tag{10}$$

where $v_{CPE1}$ is the voltage across CPE1 evaluated using 10 and $v_{CPE2}$ is likewise found for CPE2 in the equivalent circuit model.

## REFERENCES


[1] S. Westerlund and L. Ekstam, "Capacitor theory," *IEEE Trans. Dielectr. Electr. Insul.*, vol. 1, no. 5, pp. 826–839, Oct. 1994.

[2] I. Podlubny, *Fractional Differential Equations: An Introduction to Fractional Derivatives, Fractional Differential Equations, to Methods of Their Solution and Some of Their Applications*, 1st ed. New York, NY, USA: Academic, 1998.

[3] E. C. de Oliveira and J. A. Tenreiro Machado, "A review of definitions for fractional derivatives and integral," *Math. Problems Eng.*, vol. 2014, pp. 1–6, Jun. 2014.

[4] H. Fricke, "The theory of electrolytic polarization," *London, Edinburgh, Dublin Philosophical Mag. J. Sci.*, vol. 14, no. 90, pp. 310–318, 1932.

[5] J. E. B. Randles, "Kinetics of rapid electrode reactions," *Discuss. Faraday Soc.*, vol. 1, p. 11, Jan. 1947.

[6] G. Brug, "The analysis of electrode impedances complicated by the presence of a constant phase element," *J. Electroanal. Chem.*, vol. 176, nos. 1–2, pp. 275–295, Sep. 1984.

[7] U. Westerhoff, K. Kurbach, F. Lienesch, and M. Kurrat, "Analysis of lithium-ion battery models based on electrochemical impedance spectroscopy," *Energy Technol.*, vol. 4, no. 12, pp. 1620–1630, Dec. 2016.

[8] W. Choi, H.-C. Shin, J. M. Kim, J.-Y. Choi, and W.-S. Yoon, "Modeling and applications of electrochemical impedance spectroscopy (EIS) for lithium-ion batteries," *J. Electrochemical Sci. Technol.*, vol. 11, no. 1, pp. 1–13, Feb. 2020.

[9] J. Peng, J. Meng, J. Wu, Z. Deng, M. Lin, S. Mao, and D.-I. Stroe, "A comprehensive overview and comparison of parameter benchmark methods for lithium-ion battery application," *J. Energy Storage*, vol. 71, Nov. 2023, Art. no. 108197. [Online]. Available: https://www.sciencedirect.com/science/article/pii/S2352152X23015943

[10] F. Berthier, J.-P. Diard, and R. Michel, "Distinguishability of equivalent circuits containing CPEs," *J. Electroanal. Chem.*, vol. 510, nos. 1–2, pp. 1–11, Sep. 2001.

[11] E. Poihipi, J. Scott, and C. Dunn, "Distinguishability of battery equivalent-circuit models containing CPEs: Updating the work of Berthier, Diard, and Michel," *J. Electroanal. Chem.*, vol. 911, Apr. 2022, Art. no. 116201.

[12] D. Valério, M. D. Ortigueira, and A. M. Lopes, "How many fractional derivatives are there?" *Mathematics*, vol. 10, no. 5, p. 737, Feb. 2022.

[13] P. Schröer, E. Khoshbakht, T. Nemeth, M. Kuipers, H. Zappen, and D. U. Sauer, "Adaptive modeling in the frequency and time domain of high-power lithium titanate oxide cells in battery management systems," *J. Energy Storage*, vol. 32, Dec. 2020, Art. no. 101966.

[14] A. Atangana, "Fractional operators and their applications," in *Fractional Operators With Constant and Variable Order With Application to Geo-Hydrology*. New York, NY, USA: Academic, 2018, pp. 79–112.

[15] J. Sabatier, "Beyond the particular case of circuits with geometrically distributed components for approximation of fractional order models: Application to a new class of model for power law type long memory behaviour modelling," *J. Adv. Res.*, vol. 25, pp. 243–255, Sep. 2020.

[16] R. Morrison, "RC constant-argument driving-point admittances," *IRE Trans. Circuit Theory*, vol. 6, no. 3, pp. 310–317, 1959.

[17] X. Lu, H. Li, and N. Chen, "An indicator for the electrode aging of lithium-ion batteries using a fractional variable order model," *Electrochimica Acta*, vol. 299, pp. 378–387, Mar. 2019.

[18] Q. Yang, J. Xu, X. Li, D. Xu, and B. Cao, "State-of-health estimation of lithium-ion battery based on fractional impedance model and interval capacity," *Int. J. Electr. Power Energy Syst.*, vol. 119, Jul. 2020, Art. no. 105883.

[19] V. Farrow, "Characterisation of rechargeable batteries: Addressing fractional ultralow-frequency devices," M.E. thesis, Univ. Waikato, Hamilton, New Zealand, Sep. 2020. Accessed: Jan. 2021.

[20] B. Ospina Agudelo, W. Zamboni, and E. Monmasson, "A comparison of time-domain implementation methods for fractional-order battery impedance models," *Energies*, vol. 14, no. 15, p. 4415, Jul. 2021.

[21] R. Yang, R. Xiong, H. He, and Z. Chen, "A fractional-order model-based battery external short circuit fault diagnosis approach for all-climate electric vehicles application," *J. Cleaner Prod.*, vol. 187, pp. 950–959, Jun. 2018.

[22] L. Chen, Z. Lü, W. Lin, J. Li, and H. Pan, "A new state-of-health estimation method for lithium-ion batteries through the intrinsic relationship between ohmic internal resistance and capacity," *Measurement*, vol. 116, pp. 586–595, Feb. 2018.

[23] H. Mu, R. Xiong, H. Zheng, Y. Chang, and Z. Chen, "A novel fractional order model based state-of-charge estimation method for lithium-ion battery," *Appl. Energy*, vol. 207, pp. 384–393, Dec. 2017.

[24] R. Xiong, J. Tian, W. Shen, and F. Sun, "A novel fractional order model for state of charge estimation in lithium ion batteries," *IEEE Trans. Veh. Technol.*, vol. 68, no. 5, pp. 4130–4139, May 2019.

[25] N. Sene and J. F. Gómez-Aguilar, "Analytical solutions of electrical circuits considering certain generalized fractional derivatives," *Eur. Phys. J. Plus*, vol. 134, no. 6, p. 260, Jun. 2019.

[26] L. De Sutter, Y. Firouz, J. De Hoog, N. Omar, and J. Van Mierlo, "Battery aging assessment and parametric study of lithium-ion batteries by means of a fractional differential model," *Electrochimica Acta*, vol. 305, pp. 24–36, May 2019.

[27] Q. Yang, J. Xu, B. Cao, and X. Li, "A simplified fractional order impedance model and parameter identification method for lithium-ion batteries," *PLoS ONE*, vol. 12, no. 2, Feb. 2017, Art. no. e0172424.

[28] D. Andre, M. Meiler, K. Steiner, H. Walz, T. Soczka-Guth, and D. U. Sauer, "Characterization of high-power lithium-ion batteries by electrochemical impedance spectroscopy. II: Modelling," *J. Power Sources*, vol. 196, no. 12, pp. 5349–5356, Jun. 2011.

[29] X. Hu, H. Yuan, C. Zou, Z. Li, and L. Zhang, "Co-estimation of state of charge and state of health for lithium-ion batteries based on fractional-order calculus," *IEEE Trans. Veh. Technol.*, vol. 67, no. 11, pp. 10319–10329, Nov. 2018.

[30] Y. Jiang, B. Xia, X. Zhao, T. Nguyen, C. Mi, and R. A. de Callafon, "Data-based fractional differential models for non-linear dynamic modeling of a lithium-ion battery," *Energy*, vol. 135, pp. 171–181, Sep. 2017.

[31] C. R. Birkl, M. R. Roberts, E. McTurk, P. G. Bruce, and D. A. Howey, "Degradation diagnostics for lithium ion cells," *J. Power Sources*, vol. 341, pp. 373–386, Feb. 2017.

[32] J. Tian, R. Xiong, and Q. Yu, "Fractional-order model-based incremental capacity analysis for degradation state recognition of lithium-ion batteries," *IEEE Trans. Ind. Electron.*, vol. 66, no. 2, pp. 1576–1584, Feb. 2019.

[33] B. Wang, S. E. Li, H. Peng, and Z. Liu, "Fractional-order modeling and parameter identification for lithium-ion batteries," *J. Power Sources*, vol. 293, pp. 151–161, Oct. 2015.

[34] S. Li, M. Hu, Y. Li, and C. Gong, "Fractional-order modeling and SOC estimation of lithium-ion battery considering capacity loss," *Int. J. Energy Res.*, vol. 43, no. 1, pp. 417–429, Jan. 2019.

[35] K. S. R. Mawonou, A. Eddahech, D. Dumur, D. Beauvois, and E. Godoy, "Improved state of charge estimation for Li-ion batteries using fractional order extended Kalman filter," *J. Power Sources*, vol. 435, Sep. 2019, Art. no. 226710.

[36] A. N. Eddine, B. Huard, J.-D. Gabano, and T. Poinot, "Initialization of a fractional order identification algorithm applied for lithium-ion battery modeling in time domain," *Commun. Nonlinear Sci. Numer. Simul.*, vol. 59, pp. 375–386, Jun. 2018.

[37] M. Hu, Y. Li, S. Li, C. Fu, D. Qin, and Z. Li, "Lithium-ion battery modeling and parameter identification based on fractional theory," *Energy*, vol. 165, pp. 153–163, Dec. 2018.

[38] J. Sabatier, J. M. Francisco, F. Guillemard, L. Lavigne, M. Moze, and M. Merveillaut, "Lithium-ion batteries modeling: A simple fractional differentiation based model and its associated parameters estimation method," *Signal Process.*, vol. 107, pp. 290–301, Feb. 2015.

[39] Z. Chen, R. Xiong, J. Tian, X. Shang, and J. Lu, "Model-based fault diagnosis approach on external short circuit of lithium-ion battery used in electric vehicles," *Appl. Energy*, vol. 184, pp. 365–374, Dec. 2016.

[40] C. Zou, X. Hu, S. Dey, L. Zhang, and X. Tang, "Nonlinear fractional-order estimator with guaranteed robustness and stability for lithium-ion batteries," *IEEE Trans. Ind. Electron.*, vol. 65, no. 7, pp. 5951–5961, Jul. 2018.

[41] C. Fleischer, W. Waag, H.-M. Heyn, and D. U. Sauer, "On-line adaptive battery impedance parameter and state estimation considering physical principles in reduced order equivalent circuit battery models," *J. Power Sources*, vol. 260, pp. 276–291, Aug. 2014.

[42] M. Crescentini, A. De Angelis, R. Ramilli, G. De Angelis, M. Tartagni, A. Moschitta, P. A. Traverso, and P. Carbone, "Online EIS and diagnostics (don't short) on lithium-ion batteries by means of low-power integrated sensing and parametric modeling," *IEEE Trans. Instrum. Meas.*, vol. 70, pp. 1–11, 2021.
[43] J. Tian, R. Xiong, W. Shen, J. Wang, and R. Yang, "Online simultaneous identification of parameters and order of a fractional order battery model," *J. Cleaner Prod.*, vol. 247, Feb. 2020, Art. no. 119147.
[44] D. Zhou, K. Zhang, A. Ravey, F. Gao, and A. Miraoui, "Parameter sensitivity analysis for fractional-order modeling of lithium-ion batteries," *Energies*, vol. 9, no. 3, p. 123, Feb. 2016.
[45] X. Lu, H. Li, J. Xu, S. Chen, and N. Chen, "Rapid estimation method for state of charge of lithium-ion battery based on fractional continual variable order model," *Energies*, vol. 11, no. 4, p. 714, Mar. 2018.
[46] Y. Zou, S. E. Li, B. Shao, and B. Wang, "State-space model with non-integer order derivatives for lithium-ion battery," *Appl. Energy*, vol. 161, pp. 330–336, Jan. 2016.
[47] J. P. Schmidt, P. Berg, M. Schönleber, A. Weber, and E. Ivers-Tiffée, "The distribution of relaxation times as basis for generalized time-domain models for Li-ion batteries," *J. Power Sources*, vol. 221, pp. 70–77, Jan. 2013.
[48] E. Piotrowska and K. Rogowski, "Time-domain analysis of fractional electrical circuit containing two ladder elements," *Electronics*, vol. 10, no. 4, p. 475, Feb. 2021.
[49] M. R. Rapaic and A. Pisano, "Variable-order fractional operators for adaptive order and parameter estimation," *IEEE Trans. Autom. Control*, vol. 59, no. 3, pp. 798–803, Mar. 2014.
[50] J. Scott and R. Hasan, "New results for battery impedance at very low frequencies," *IEEE Access*, vol. 7, pp. 106925–106930, 2019.
[51] C. Dunn and J. Scott, "Achieving reliable and repeatable electrochemical impedance spectroscopy of rechargeable batteries at extra-low frequencies," *IEEE Trans. Instrum. Meas.*, vol. 71, pp. 1–8, 2022.
[52] C. Dunn, J. Scott, M. Wilson, M. Cree, and M. Mucalo, "Cyclic voltammetry of batteries and implications for reliable electrochemical impedance spectroscopy," Jan. 2023, doi: 10.2139/ssrn.4401777.
[53] S. G. Samko, A. A. Kilbas, and O. I. Marichev, *Fractional Integrals Derivatives*, vol. 1. Yverdon Yverdon-Les-Bains, Switzerland: Gordon and Breach Science Publishers, 1993.

**VANCE FARROW** received the B.E. (Hons.) and M.E. degrees in electronic engineering with The University of Waikato, Hamilton, New Zealand, in 2019, where he is currently pursuing the Ph.D. degree, working on battery management systems using fractional-derivative models and extremely low frequency electrochemical impedance spectroscopy measurements. His M.E. focused on the prediction of battery life using small-signal measurements.

**JONATHAN SCOTT** (Life Senior Member, IEEE) received the B.Sc., B.E. (Hons.), M.Eng.Sc., and Ph.D. degrees from The University of Sydney, Sydney, NSW, Australia, in 1977, 1979, 1985, and 1997, respectively, and the PGC Management in higher education from Waikato University, in 2014. From 1997 to 1998, he was the Chief Engineer of RF Technology, Sydney. He was with the Department of Electrical Engineering, The University of Sydney, prior to 1997. From 1998 to 2006, he was with Hewlett-Packard and Agilent Technologies Microwave Technology Center, Santa Rosa, CA, USA, where he was responsible for advanced measurement systems operating from dc to millimeter-wave. He was the Foundation Professor of electronic engineering with The University of Waikato, Hamilton, New Zealand, from 2006 to 2022. He has authored more than 150 refereed publications, several book chapters, and a textbook. He holds numerous patents, several covering active products from microwave and RF to biomedical and battery systems. His educational interests include threshold concepts and their application, particularly across engineering disciplines. His research interests include the characterization and modeling of implantable electrodes, semiconductor devices, batteries, and acoustic systems.

**MICHAEL J. CREE** (Senior Member, IEEE) received the B.Sc. (Hons.) and Ph.D. degrees from the University of Canterbury, in 1990 and 1994, respectively. He is currently an Associate Professor of electrical and electronic engineering with The University of Waikato, Hamilton, New Zealand. His research interests include medical imaging, computer vision, time-of-flight range imaging, and more recently batteries. He is a Co-Editor of *Automated Image Detection of Retinal Pathology*, in 2010.

**MARCUS WILSON** received the degree (Hons.) in physics and theoretical physics from the University of Cambridge, in 1992, and the Ph.D. degree in theoretical solid state physics from the University of Bristol, in 1995. He is currently a Senior Lecturer in physics and chemistry with Te Aka Mātuatua – School of Science, The University of Waikato, Hamilton, New Zealand. He has worked in numerical modeling of physics processes in industry, U.K. and in academia, New Zealand, since 2004. His research interests include electric properties and dynamics of the human brain, transcranial magnetic stimulation, and more recently batteries.